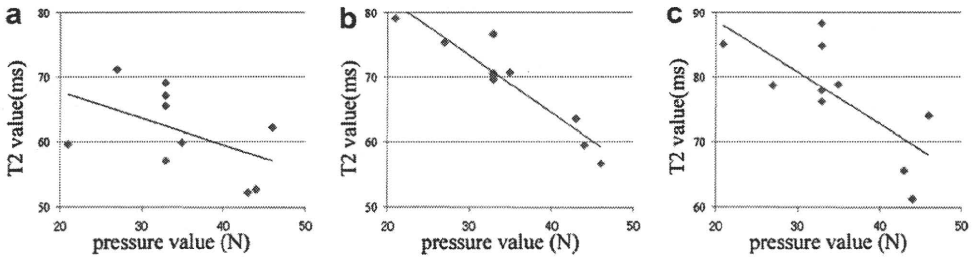

Fig. 7. The correlation between T2 values and contact pressure in the lateral cartilage on varus loading. (a) deep zone (b) intermediate zone (c) superficial zone.

to loading was mostly achieved in a short duration in the present study. A relatively low magnitude of applied load (approximately one-third of the body weight) may shorten the duration to reach the final equilibrium condition of cartilage deformation.

Our study had several limitations. First, the cartilage boundary for ROI placements was manually defined for calculation of cartilage T2. However, cartilage boundary was easily determined presumably because of the relatively high in-plane resolution, high signal contrast between the cartilage and adjacent subchondral bone, and use of anterior and posterior menisci as anatomical landmarks. The intra-observer and inter-observer reproducibility of cartilage T2 measurements in the present study ranged from 3% to 5% at each zone, which was comparable to results obtained in previous studies[13,31]. We detected significant decreases in cartilage T2 values at intermediate zone under neutral loading-1 and varus loading, which were more than the double of the reproducibility of T2 measurements. Given the acceptable reproducibility of the present measurements to detect significant change of cartilage T2 by loading, we consider that ROIs were reliably defined in the present study. Second, the composition and thickness of the articular cartilage in different species may vary with different load-bearing patterns, and the *ex vivo* whole-knee model did not take into account surrounding muscle action (e.g., contraction of quadriceps or hamstrings) or forces from surrounding ligamentous restraints. Severity and localization of change in the MRI measurements in association with loading or varus alignment may be different in human knee imaging *in vivo*. In the present study, distribution patterns of T2 mapping with lower T2 in the deep zone and higher T2 in the superficial zone without loading were similar to those of human adult cartilage *in vivo*[32,33]. We believe that this model had a water distribution pattern similar to human cartilage and allowed investigation of the load response of cartilage extracellular matrix mainly with respect to water distribution by T2 mapping. Third, although time-dependent compressive creep and stress relaxation behavior of cartilage occur in the biphasic theory[34], we validated accuracy of the device using an incompressible rod because a testing material which had biomaterial property similar to viscoelastic property of cartilage was not available. In the present study, the analysis of the cartilage deformation of the weight-bearing area in the SPGR image corresponding T2 map showed mean reduction of approximately 0.2 mm thickness under neutral loading-1, and approximately 0.4 mm thickness under varus loading compared with the initial thickness. Compression of viscoelastic foam material by 10 mm resulted in providing continuous compression force to the incompressible rod by 134 N–140 N. Loss of compression of the foam material by 0.4 mm due to cartilage deformation was assumed to decrease the compression force about 4.8 N from additional experiments (data was not shown). As the cartilage deformation of viscoelastic phenomena was relatively small compared with the displacement of the foam material, we considered the result of the preliminary test with incompressible rod provided similar results regarding the accuracy of the device. Fourth, cartilage T2 was evaluated under viscoelastic phenomena such as stress relaxation, but the pressure-sensitive film left inside a joint recorded the peak pressures during the loading period. Although real-time measurement of pressure was impossible for the pressure-sensitive film, this film has advantages in matching the sheet form to convex of the knee joint and minimizing change of biomechanical condition by placing the thin film into the knee joint. With this limitation in mind, we investigated how femoral cartilage T2 changed in layer-specific manner using the realistic whole-knee joint model when cartilage surface was compressed by static loading and varus knee alignment condition. Care should be taken for interpretation of the present finding that direct correlation between depth-wise distribution of strain and T2 value within the cartilage was not clarified in this study. Finally, we also have interest on analysis of T2 changes of the tibial cartilage in association with the opposing femoral cartilage when the load is applied. However, comparison of the T2 mapping in the same location of the tibial cartilage between the neutral loading and varus loading might be difficult because it was difficult to place the same saggital imaging plane in the oblique-positioned tibia at varus loading, to the imaging plane in the neutral-positioned tibia. In contrast, the position of the femur was constant throughout the experiment (no loading, neutral loading and varus loading). In our layer-specific analysis of cartilage T2, ROI placement in the same anatomical location was important to reveal accurate change of T2 value in association with loading conditions. Furthermore, thickness of the tibial cartilage, ranging 1 mm–2 mm, was small as compared with the femoral cartilage thickness ranging 3 mm–4 mm. In the present study, in-plane resolution of T2 maps was 0.26 mm × 0.39 mm. Due to thin thickness, we consider that adequate evaluation of T2 values in the three subdivided layers along the cartilage depth was difficult in the tibial cartilage. From these concerns, we focused on analysis of T2 changes of the femoral cartilage in the present study.

In conclusion, our results indicated that quantitative assessment of MRI for the cartilage differed in various physiological conditions, and T2 mapping under static loading allowed non-invasive biomechanical assessment of site-specific stress distribution in the cartilage. Although further investigations will be required, evaluation of dynamic changes in the collagen architecture, along with evaluation of water influx or efflux through the cartilage in response to physiological loading, may provide more sensitive and detailed assessment of degenerative pathological changes and load-bearing function of the cartilage compared to mere static assessment of solid matrix and water content.

Conflict of interest

The authors have no conflict of interest.

Acknowledgments

The authors wish to thank Yasuo Hara, Department of Technology Development, IVTeC, Japan, for technical assistance, and Ichiro Nakahara, Department of Orthopaedic Surgery, Osaka

University Medical School, Osaka, Japan, for his assistance in image analysis.

This work was supported in part by a program "Collaborative Development of Innovative Seeds" (6090026) from the Japan Science and Technology Agency and Grant-in-Aid for Scientific Research (19591757) of the Ministry of Education, Science and Culture in Japan.

References

1. Mosher TJ, Dardzinski BJ, Smith MB. Human articular cartilage: influence of aging and early symptomatic degeneration on the spatial variation of T2-preliminary findings at 3 T. Radiology 2000;214:259–66.
2. Dunn TC, Lu Y, Jin H, Ries MD, Majumdar S. T2 relaxation time of cartilage at MR imaging: comparison with severity of knee osteoarthritis. Radiology 2004;232:592–8.
3. Burstein D, Bashir A, Gray ML. MRI techniques in early stages of cartilage disease. Invest Radiol 2000;35:622–38.
4. Li X, Benjamin M, Link TM, Castillo DD, Blumenkrantz G, Lozano J, *et al. In vivo* $T_{1\rho}$ and T_2 mapping of articular cartilage in osteoarthritis of the knee using 3 T MRI. Osteoarthritis Cartilage 2007;15:789–97.
5. Li X, Pai A, Blumenkrantz G, Carballido-Gamio J, Link T, Benjamin C, *et al.* Spatial distribution and relationship of $T_{1\rho}$ and T_2 relaxation times in knee cartilage with osteoarthritis. Magn Reson Med 2009;61:1310–8.
6. Mosher TJ, Smith HE, Collins C, Liu Y, Hancy J, Dardzinski BJ, *et al.* Change in knee cartilage T2 at MR imaging after running: a feasibility study. Radiology 2005;234:245–9.
7. Eckstein F, Tieschky M, Faber SC, Haubner M, Kolem H, Englmeier KH, *et al.* Effect of physical exercise on cartilage volume and thickness *in vivo*: MR imaging study. Radiology 1998;207:243–8.
8. Gründer W, Kanowski M, Wagner M, Werner A. Visualization of pressure distribution within loaded joint cartilage by application of angle-sensitive NMR microscopy. Magn Reson Med 2000;43:884–91.
9. Rubenstein JD, Kim JK, Henkelman RM. Effects of compression and recovery on bovine articular cartilage: appearance on MR images. Radiology 1996;201:843–50.
10. Herberhold C, Faber S, Stammberger T, Steinlechner M, Putz R, Englmeier KH, *et al.* In situ measurement of articular cartilage deformation in intact femoropatellar joints under static loading. J Biomech 1999;32:1287–95.
11. Kaufman JH, Regatte RR, Bolinger L, Kneeland JB, Reddy R, Leigh JS. A novel approach to observing articular cartilage deformation *in vitro via* magnetic resonance imaging. J Magn Reson Imaging 1999;9:653–62.
12. Menezes NM, Gray ML, Hartke JR, Burstein D. T_2 and $T_{1\rho}$ MRI in articular cartilage systems. Magn Reson Med 2004;51: 503–9.
13. Liess C, Lüsse S, Karger N, Heller M, Glüer CC. Detection of changes in cartilage water content using MRI T2-mapping *in vivo*. Osteoarthritis Cartilage 2002;10:907–13.
14. Hayashi K, Takano H, Matsuda T, Umezu M. Mechanical stability of elastomeric polymers for blood pump applications. J Biomed Mater Res 1985;19:179–93.
15. Fukubayashi T, Kurosawa H. The contact area and pressure distribution of the knee. Acta Orthop Scand 1980;51:871–9.
16. Wu JZ, Herzog W, Epstein M. Effects of inserting a pressensor film into articular joints on the actual contact mechanics. J Biomech Eng 1998;120:655–9.
17. Wayne JS, Kraft KA, Shields KJ, Yin C, Owen JR, Disler DG. MR imaging of normal and matrix-depleted cartilage: correlation with biomechanical function and biochemical composition. Radiology 2003;228:493–9.
18. Nishii T, Kuroda K, Matsuoka Y, Sahara T, Yoshikawa H. Change in knee cartilage T2 in response to mechanical loading. J Magn Reson Imaging 2008;28:175–80.
19. Nag D, Liney GP, Gillespie P, Scerman KP. Quantification of T2 relaxation changes in articular cartilage with in situ mechanical loading of the knee. J Magn Reson Imaging 2004;19:317–22.
20. Donnan FG. The theory of membrane equilibria. Chem Rev 1924;1:73–90.
21. Maroudas A, Schneiderman R. "Free" and "exchangeable" or "trapped" and "non-exchangeable" water in cartilage. J Orthop Res 1987;5:133–8.
22. Rubenstein JD, Kim JK, Morova-Protzner I, Stanchev PL, Henkelman RM. Effects of collagen orientation on MR imaging characteristics of bovine articular cartilage. Radiology 1993;188:219–26.
23. Peto S, Gillis P. Fiber-to-field angle dependence of proton nuclear magnetic relaxation in collagen. Magn Reson Imaging 1990;8:705–12.
24. Reiter DA, Lin PC, Fishbein KW, Spencer RG. Multicomponent T2 relaxation analysis in cartilage. Magn Reson Med 2009;61:803–9.
25. Hardy PA, Ridler AC, Chiarot CB, Plewes DB, Henkelman RM. Imaging articular cartilage under compression – cartilage elastography. Magn Reson Med 2005;53:1065–73.
26. Eckstein F, Wirth W, Hudelmaier M, Stein V, Lengfelder V, Cahue S, *et al.* Patterns of femorotibial cartilage loss in knees with neutral, varus, and valgus alignment. Arthritis Rheum 2008;59:1563–70.
27. Morrison JB. The mechanics of the knee joint in relation to normal walking. J Biomech 1970;3:51–61.
28. Harrington IJ. Static and dynamic loading patterns in knee joints with deformities. J Bone Joint Surg Am 1983;65: 247–59.
29. Visser SK, Crawford RW, Pope JM. Structual adaptations in compressed articular cartilage measured by diffusion tensor imaging. Osteoarthritis Cartilage 2008;16:83–9.
30. Guettler J, Glisson R, Stubbs A, Jurist K, Hoggins L. The triad of varus malalignment, meniscectomy, and chondral damage: a biomechanical explanation for joint degeneration. Orthopedics 2007;30:558–66.
31. Glaser C, Mendlik T, Dinges J, Weber J, Stahl R, Trumm C, *et al.* Global and regional reproducibility of T2 relaxation time measurements in human patellar cartilage. Magn Reson Med 2006;56:527–34.
32. Nishii T, Tanaka H, Sugano N, Sakai T, Hananouchi T, Yoshikawa H. Evaluation of cartilage matrix disorders by T2 relaxation time in patients with hip dysplasia. Osteoarthritis Cartilage 2008;16:227–33.
33. Smith HE, Mosher TJ, Dardzinski BJ, Collins BG, Collins CM, Yang QX, *et al.* Spatial variation in cartilage T2 of the knee. J Magn Reson Imaging 2001;14:50–5.
34. Mow VC, Kuei SC, Lai WM, Armstrong CG. Biphasic creep and stress relaxation of articular cartilage in compression? Theory and experiments. J Biomech Eng 1980;102:73–84.

Magnetic Resonance in Medicine 64:707–714 (2010)

Influence of Knee Positions on T_2, T^*_2, and dGEMRIC Mapping in Porcine Knee Cartilage

Toshiyuki Shiomi,[1] Takashi Nishii,[1,2]* Akira Myoui,[1,3] Hideki Yoshikawa,[1] and Nobuhiko Sugano[1,2]

We examined the influence of flexed knee positions on cartilage MR assessments. Sagittal T_2, T^*_2, and delayed gadolinium-enhanced MRI of cartilage (dGEMRIC) maps of the femoral cartilage were obtained in eight 6-month-old porcine femorotibial joints in the extended knee position (position A: flexion 0° and femoral shaft in parallel with the amplitude of static field), flexed knee position (position B: flexion 40° and femoral shaft oriented at 40° to the amplitude of static field), and oblique-placed knee-extended position (position C: flexion 0° and femoral shaft oriented at 40° to the amplitude of static field). Comparison of the MR parameters between positions A and C showed isolated influence of the magic-angle effect, and comparison between positions A and B showed effects of knee flexion. Proteoglycan and hydroxyproline content in cartilage specimen at each region of interest had no significant correlation with T_2, T^*_2, and dGEMRIC values. At the central zone, located on a weight-bearing area and parallel to the amplitude of static field, T_2/T^*_2/dGEMRIC values increased by 6.8/11/0.8% at position C and by 24/44/31% at position B compared with position A. There was a significant increase in T_2 and T^*_2 values at position B compared with those at position A. The substantial changes in T_2, T^*_2, and dGEMRIC were shown in response to knee flexion, presumably due to the compounding influence of the magic-angle effect and change in the intra-articular biomechanical condition. Magn Reson Med 64:707–714, 2010. © 2010 Wiley-Liss, Inc.

Key words: MRI; knee cartilage; T_2; T^*_2; dGEMRIC

Knee imaging using quantitative MRI techniques, such as T_2 (1,2), T^*_2 (3), delayed gadolinium-enhanced MRI of cartilage (dGEMRIC) (4,5), and T_1 in the rotating frame (T1rho) (6), achieved great advancements in noninvasive assessments of the articular cartilage, particularly about matrix compositions and degenerative changes. Sensitive evaluations in water, collagen, or proteoglycan content and collagenous arrangements in the cartilage in vivo were obtained using the aforementioned techniques, without performing destructive retrieval analysis.

In most clinical studies, quantitative MR assessments were performed in the extended knee position, with the longitudinal axis of the femur and tibia aligned in parallel with the amplitude of static magnetic field (B_0). Recently, knee kinematic investigations using MRI at flexion in various angles have provided valuable information regarding the physiological and pathological conditions of intra-articular structures and their varied interactions among the articular cartilage, meniscus, and ligaments (7,8). Flexion of the knee joints resulted in a significantly different tibiofemoral contact area between healthy and injured knee joints, depending on the flexion angle. In such cases, by reflecting on the concomitant change of water content or deformation of collagenous arrangements in the cartilage (9–11), quantitative MR techniques may be effective for evaluating the biomechanical environment of articular cartilage in association with knee movements.

Quantitative MR evaluation in knee kinematic investigations, however, may encounter difficulties due to the magic-angle effect. Angular changes in the femoral and tibial positioning with respect to B_0 may cause a substantial localized change in the MR signal intensity due to the magic-angle effect. In prior experimental studies using excised cartilage specimens, a strong orientation dependence on the relaxation time of articular cartilage in MRI, especially for T_2, was observed (12). Maximum effect of T_2 elongation was obtained when the collagen fibers in the cartilage were oriented at ~55° relative to B_0. Clinically, focally increased signals observed on short echo time images of cartilage with curved articular surfaces such as the femoral condyle were partly accounted for by the magic-angle effect. Therefore, it may be difficult to distinguish between the changes in quantitative MR assessments of the femoral cartilage associated with knee flexion due to alteration of content or structure in water or extracellular matrix within the cartilage and those caused by the magic-angle effect.

Previous experimental investigations using isolated, excised cartilage specimens explored the effect of magic angle on MR relaxation time in detail. To our knowledge, however, no studies have documented an orientation dependence of cartilage relaxation time associated with the flexion of the knee in clinical situations, with a whole joint model retaining the meniscus, ligaments, and the capsule in situ. The purpose of this study is to examine the influence of flexed knee positions on cartilage assessments by T_2, T^*_2, and dGEMRIC mapping, using cadaver porcine femorotibial joints, and to correlate articular

[1]Department of Orthopaedic Surgery, Osaka University Medical School, Osaka, Japan.

[2]Department of Orthopaedic Medical Engineering, Osaka University Medical School, Osaka, Japan.

[3]Medical Center for Translational Research, Osaka University Hospital, Osaka, Japan.

Grant sponsor: Japan Science and Technology Agency; Grant number: 6090026 (Collaborative Development of Innovative Seeds program); Grant sponsor: Ministry of Education, Science and Culture in Japan; Grant number: 19591757.

*Correspondence to: Takashi Nishii, M.D., Department of Orthopaedic Medical Engineering, Osaka University Medical School, 2-2 Yamadaoka, Suita, Osaka 565-0871, Japan. E-mail: nishii@ort.med.osaka-u.ac.jp

Received 11 March 2009; revised 5 February 2010; accepted 7 March 2010.

DOI 10.1002/mrm.22469

Published online 9 June 2010 in Wiley Online Library (wileyonlinelibrary.com).

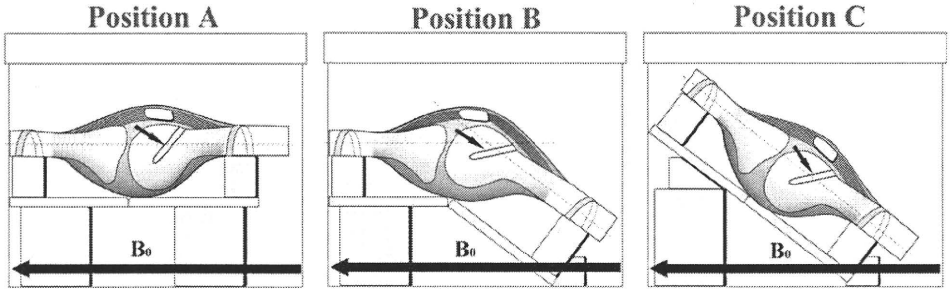

FIG. 1. Femorotibial porcine knee joints in the extended knee position (position A: flexion 0° and the femoral shaft in parallel with B_0), flexed knee position (position B: flexion 40° and the femoral shaft oriented at 40° to B_0), and oblique-placed knee-extended position (position C: flexion 0° and the femoral shaft oriented at 40° to B_0). A small cylindrical bone defect (arrow) was made in the middle of the lateral and medial femoral condyle as a fiducial mark.

biochemical compositions, such as proteoglycan and collagen content, in MRI parameters.

MATERIALS AND METHODS

Preparation of Porcine Specimens

Eight fresh knee joints were harvested en bloc with intact capsule and surrounding muscle from 6-month-old pigs and stored at −40°C. On the day of MRI, the specimens were thawed at room temperature and a small cylindrical bone defect was made in the middle of the lateral and medial femoral condyle as a fiducial mark. First, the muscle was stripped from the anterior side of the femoral shaft up to the upper end of the femoral condyle and the bone defect was made using a 3 mm-diameter from the upper anterior end to the center portion of the femoral condyle. The defect did not reach the femoral articular cartilage and the subchondral bone to eliminate an artificial effect on MRI by the scar. Then, a wooden stick of the corresponding size was introduced into the bone defect. This bone defect was used to obtain reproducible identification of the same imaging plane and for defining the regions of interest (ROIs) in subsequent imaging sequences. During the procedure, care was taken to preserve the capsule and the medial and lateral collateral ligament around the knee joint. The specimen was fixed in an acryl box filled with phosphate-buffered saline, and the air in the box was removed. The knee joint, sealed by the capsule, was also filled with phosphate-buffered saline by injection via the capsule.

MRI

MRI was performed using a 1.5-T MRI system (MAGNETOM Espree; Siemens, Erlangen, Germany) and a standard 14-cm-diameter quadrature knee coil (Siemens). The MR system was equipped with 4×10^{-4} T/cm gradients. The porcine knee was placed in a supine, head-first orientation in the center of the coil. Sagittal T_2 and T_2^* maps were first obtained for the lateral and medial femorotibial joints in the extended knee position (position A: flexion 0° and the femoral shaft in parallel with B_0) and then in the flexed knee position (position B: flexion ~40° and the femoral shaft, oriented at 40° to B_0) (Fig. 1). In both knee positions, the tibia was placed in parallel with B_0. A flexion angle of 40° was confirmed, using a measurement device. During analyses of the MR images, the actual flexion angle at position B averaged 41.5° ± 2.5°. Then, the knee joints were immersed and equilibrated in 1-mM gadolinium-diethylene triamide pentaacetic acid solution (Magnevist; Schering AG, Germany) for 3 h. We determined the immersion time based on previous studies (13,14) in which nearly maximal increase of T_1-weighted signal intensity was obtained by 2.5-h immersion of cartilage specimen in gadolinium-diethylene triamide pentaacetic acid solution. Then, sagittal dGEMRIC maps were obtained in the same imaging plane and knee positions (positions A and B). In all mappings, the corresponding sagittal plane was determined to include the fiducial mark.

In six of the eight knees, the sagittal T_2, T_2^*, and dGEMRIC maps in the extended knee position (flexion 0°) and the femoral shaft oriented at 40° to B_0 (position C) were also obtained to evaluate the isolated influence of the magic-angle effect (Fig. 1).

T_2 and T_2^* maps were calculated using a monoexponential fit from two-dimensional multiecho spin-echo sequences (pulse repetition time, 4000 msec; 10 echoes between 18.7 and 187 msec; field of view, 10 cm; matrix, 256 × 256; slice thickness, 3 mm; signal averaging, 2; acquiring time, 13 min 9 sec) and two-dimensional multiecho gradient echo sequences (pulse repetition time, 1500 ms; nine echoes between 10 and 72.96 msec; field of view, 10 cm; matrix, 256 × 256; slice thickness, 3 mm; signal averaging, 2; acquiring time, 6 min 24 sec), respectively. Frequency-selective fat-suppression technique was used to minimize the chemical shift artifact at the cartilage–bone interface. Frequency encoding was oriented in the cranial-to-caudal direction. In a preliminary experiment using 10 excised distal femurs of juvenile pigs, we compared T_2 measurements on several ROIs of the femoral cartilage with and without fat-suppression technique. The frequency-selective fat-suppression technique had no significant influence on T_2 measurements on the femoral cartilage. dGEMRIC maps were calculated from an inversion-recovery fast spin-echo sequence (pulse repetition time, 1800 ms; echo time, 14 ms; inversion time = 50–1680 msec; echo train length, 5; field of

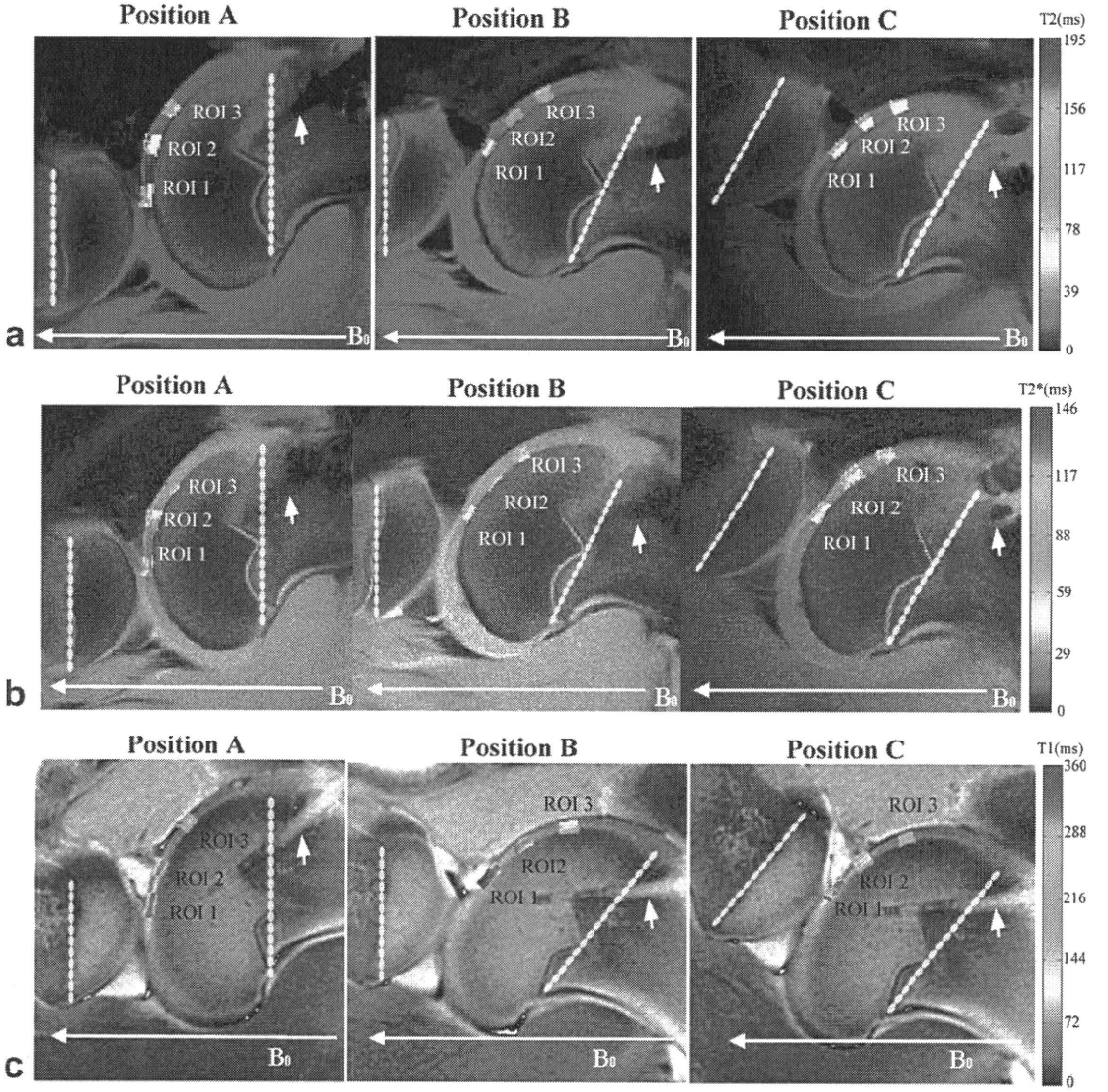

FIG. 2. Sagittal T_2 (a), T_2^*(b), and dGEMRIC (c) maps, respectively, with definition of ROIs 1, 2, and 3 at positions A, B, and C. White arrowheads indicate fiducial marks. Dotted lines are perpendicular to the femoral and tibial shaft.

view, 10 cm; matrix, 256 × 256; slice thickness, 3 mm; signal averaging, 2; acquiring time, 11 min 5 sec). In all sequences, one sagittal image passing through the middle of the medial femoral condyle and one sagittal image passing through the middle of the lateral femoral condyle with the fiducial marks were obtained. All data analyses were conducted using in-house MatLab scripts (MathWorks Inc., Natick, MA).

Image Analysis

In each mapping at knee position A, three ROIs were manually defined on the medial and lateral femoral cartilages (Fig. 2): ROI 1 was covered by the anterior meniscus in the weight-bearing area and was parallel to B_0, and ROIs 2 and 3 were free from the weight-bearing area and oriented at 25° and 50° to B_0, respectively. Placement of the three ROIs in the mappings at knee positions B and C were matched with the ROIs at knee position A, using the fiducial mark. Definitions of ROIs were repeated twice by a single observer (T.S.), and the T_2, T_2^*, and dGEMRIC values of each medial and lateral ROI were averaged. The values of ROI 2 from the lateral femoral condyle were excluded from the analysis because the region was anatomically covered with fibrous tissue. Reproducibility between the two measurements was calculated as the coefficient of variation (standard deviation/mean × 100%), and mean reproducibility was calculated as the root mean square average for all specimens. Reproducibility at each ROI ranged from 3.5 to 5.0% in T_2, 3.9 to 5.6% in T_2^*, and 3.5 to 5.0% in dGEMRIC measurements. To investigate influence of equilibration time for dGEMRIC assessment in en bloc knee joints, dGEMRIC values were measured repeatedly after immersion in 1-mM gadolinium-diethylene triamide pentaacetic acid solution both for 3 h and 24 h in another two porcine knee joints.

T_2, T_2^*, and dGEMRIC values for extended (position A) and flexed (position B) knee positions at each ROI were compared using the Wilcoxon test to estimate the

Table 1
T_2, T_2^*, and dGEMRIC Values in Each ROI (Mean ± SD) at Knee Positions A and B ($N = 8$)*

Zones		Position A	Position B	Change (%)	P value
T_2 value (msec)	ROI 1	80.7 ± 8.8	97.9 ± 16.5	24.1 ± 27.9	0.014[a]
	ROI 2	98.6 ± 11.6	98.5 ± 12.2	0.1 ± 6.7	0.128
	ROI 3	112.7 ± 25.4	88.9 ± 17.5	−17.9 ± 19.2	0.004[a]
T_2^* value (msec)	ROI 1	33.0 ± 9.7	44.3 ± 8.2	44.4 ± 47.3	0.002[a]
	ROI 2	46.0 ± 9.5	58.5 ± 7.2	29.9 ± 20.4	0.012[a]
	ROI 3	52.6 ± 17.8	49.6 ± 14.7	−2.9 ± 23.4	0.379
dGEMRIC value (msec)	ROI 1	166.3 ± 80.5	188.0 ± 65.4	30.6 ± 69.2	0.277
	ROI 2	244.3 ± 86.3	239.1 ± 58.1	2.8 ± 18.9	0.674
	ROI 3	277.1 ± 64.3	244.6 ± 62.3	−10.5 ± 18.4	0.234

*Changes were calculated as (values at position B − values at position A)/values at position A × 100.
[a]Significant difference between values at positions A and B.

influence of posture change that occurs naturally during clinical examinations. MR quantitative values with knee extension at positions A and C at each ROI were compared using the Wilcoxon test to estimate the isolated influence of the magic-angle effect that occurs due to a relative change in the femoral articular cartilage against B_0. Relationships among changes in the T_2, T_2^*, and dGEMRIC values associated with knee flexion were evaluated using the Spearman correlation coefficient. A probability value of $P < 0.05$ was considered statistically significant.

Biochemical Analysis

After MRI, a biochemical assay of the cartilage specimen at each ROI was performed to determine the proteoglycan and collagen content. Using a cylindrical punch, full-thickness cartilage disks (diameter of 4 mm) without subchondral bone were removed from the knees, matching each ROI. The cartilage was analyzed to determine the concentrations of hydroxyproline, a measure of collagen content, and sulfated glycosaminoglycan, a measure of proteoglycan content. For assessment of hydroxyproline content, the cartilage was hydrolyzed with 6-N hydrochloric acid at 130°C for 6 h, neutralized, and analyzed using a colorimetric procedure at a wavelength of 557 nm. For analysis of sulfated glycosaminoglycan content, the cartilage was digested in papain solution and then assessed using the dimethylmethylene blue binding assay at a wavelength of 535 nm.

Polarized Light Microscopy

Histological assessment of birefringence in 6-month-old porcine femoral cartilage specimens was conducted using polarized light microscopy. Birefringence of articular cartilage is suggested to be an index of the combined effect of collagen content and network organization (15). Polarized light microscopy measurement was conducted using a VHX-1000 digital microscope (Keyence, Japan) equipped with a VH-Z100UW universal zoom lens (Keyence). To determine collagen anisotropy, a cartilage sample, which was formalin fixed and treated with enzymatic removal of proteoglycans and cut into 5-μm-thick microscopic sections, was imaged at various orientations of crossed polarizers, and the maximum contrast of birefringence was recorded.

RESULTS

In the investigation for influence of equilibration time for dGEMRIC assessment, the average dGEMRIC values of ROIs 1/2/3 for the lateral and medial femorotibial joints were 174/193/206 msec at 3-h immersion and 171/182/201 msec at 24-h immersion. Immersion in contrast agent for 3 h was assumed to be sufficient to equilibrate the articular cartilage of en bloc knee joints in dGEMRIC assessment.

Table 1 shows T_2, T_2^*, and dGEMRIC values in each ROI between knee position A and position B, and Table 2 shows those values between knee position A and position C. At position A, the average quantitative values of ROIs 1/2/3 were 81/99/113 msec for T_2, 33/46/53 msec

Table 2
T_2, T_2^*, and dGEMRIC Values in Each ROI (Mean ± SD) at Knee Positions A and C ($N = 6$)*

Zones		Position A	Position B	Change (%)	P value
T_2 value (msec)	ROI 1	81.3 ± 15.0	84.7 ± 10.1	6.8 ± 19.7	0.374
	ROI 2	95.2 ± 8.5	99.7 ± 10.4	5.2 ± 11.9	0.074
	ROI 3	105.2 ± 22.3	90.5 ± 12.4	−12.1 ± 13.2	0.012[a]
T_2^* value (msec)	ROI 1	30.6 ± 9.6	33.5 ± 11.8	11.2 ± 23.3	0.224
	ROI 2	43.5 ± 6.5	50.2 ± 11.0	15.1 ± 16.5	0.075
	ROI 3	47.8 ± 15.6	43.8 ± 13.9	−6.7 ± 13.7	0.077
dGEMRIC value (msec)	ROI 1	179.8 ± 84.1	179.4 ± 84.0	0.8 ± 13.9	0.875
	ROI 2	233.7 ± 98.3	228.5 ± 89.7	−1.4 ± 8.3	0.753
	ROI 3	264.7 ± 58.5	229.3 ± 61.7	−11.4 ± 20.4	0.084

*Changes were calculated as (values at position C − values at position A)/values at position A × 100.
[a]Significant difference between values at positions A and C.

Table 3
The Proteoglycan and Hydroxyproline Content (Mean ± SD) and Correlation Coefficient With T_2, T_2^*, and dGEMRIC in Each ROI*

Cartilage matrix		ROI 1	ROI 2	ROI 3
Proteoglycan	Content (μg/mg)	57.0 ± 8.8	56.1 ± 10.1	55.9 ± 6.4
	Correlation with T_2	0.15	0.28	−0.24
	Correlation with T_2^*	0.28	0.15	−0.35
	Correlation with dGEMRIC	0.28	0.18	−0.27
Hydroxyproline	Content (μg/mg)	116.6 ± 12.4	116.9 ± 10.9	119.6 ± 10.8
	Correlation with T_2	0.20	0.21	0.21
	Correlation with T_2^*	0.20	0.03	−0.03
	Correlation with dGEMRIC	0.15	−0.65	−0.38

*No significant correlation between cartilage matrix and T_2/T_2^*/dGEMRIC values in all ROIs.

for T_2^*, and 166/244/277 msec for dGEMRIC values (Table 1). T_2, T_2^*, and dGEMRIC values in the anteriorly located zones (ROIs 2 and 3) had significantly higher values ($P < 0.05$) compared with those in the centrally located zone (ROI 1). Relative to the values at ROI 1, there was an increase of 22% at ROI 2 and 40% at ROI 3 on average T_2 values, an increase of 39% at ROI 2 and 61% at ROI 3 on average T_2^* values, and an increase of 47% at ROI 2 and 67% at ROI 3 on average dGEMRIC values. T_2 value was significantly correlated with that of T_2^*, with the correlation coefficient being 0.6 ($P < 0.01$) at ROI 1, 0.4 ($P < 0.05$) at ROI 2, and 0.6 ($P < 0.05$) at ROI 3. However, dGEMRIC value had no significant correlation with T_2 and T_2^* values at each zone.

The average proteoglycan and hydroxyproline content in each ROI was 57/56/56 μg/mg and 117/117/120 μg/mg, respectively (Table 3). There were no significant differences in the proteoglycan and hydroxyproline contents among ROIs, and these values were not correlated with T_2, T_2^*, and dGEMRIC values, using the Spearman correlation coefficient (Table 3).

At position B, T_2/T_2^*/dGEMRIC values increased by 24/44/31% at ROI 1 and decreased by 18/2.9/11% at ROI 3 on average compared with the values at position A (Table 1). There was a significant increase in the T_2 value at ROI 1 and the T_2^* value at ROIs 1 and 2 and a significant decrease in the T_2 value at ROI 3 ($P < 0.05$).

At position C, the T_2/T_2^*/dGEMRIC values increased by 6.8/11/0.8% at ROI 1 and decreased by 12/6.7/11% at ROI 3 on average compared with the values at position A (Table 2). There was no significant difference in the T_2/T_2^*/dGEMRIC values between positions A and C except a significant decrease in the T_2 value at ROI 3 ($P < 0.05$).

In the polarized light microscopy assessment, the cartilage of 6-month-old pigs had two zones with different birefringence intensity. As the birefringence is caused by a considerable influence of collagen network arrangement on the cartilage matrix structure, the result indicated that the porcine cartilage used in this study had anisotropic collagen structure (Fig. 3).

DISCUSSION

In biological tissues with highly ordered collagen, such as tendons and ligaments, strong parallel-oriented dipolar interactions of protons in water molecules binding to collagen make a significant contribution in dephasing the MR signal after excitation, resulting in shortened T_2 (16,17). The dipolar interactions are modulated by the angle between the vector joining the two spins and the external magnetic field and are minimized when the angle approaches 55° (called the magic angle), leading to a relative increase of T_2 compared with other angles of the direction. Quantitative MR evaluation of the articular cartilage is also subject to influence of the magic-angle effect, in accordance with the relative position between the collagen alignment of the cartilage and the direction of external magnetic field (18). The ultrastructure of a normal cartilage represents anisotropic collagen fiber architecture along its depth. The presence of 40–60% of deep cartilage represents predominantly parallel orientation of the fiber perpendicular to the subchondral plate (radial zone). The next 20–30% of the cartilage represents random orientation of the fiber (transitional zone). The thin superficial zone with 3–12% of the cartilage represents alignment of the collagen parallel to the articular surface (16). Previous experimental studies using excised cartilage specimen showed different magnitudes of the magic-angle effect, depending on the depth of the cartilage due to variability in the arrangement of collagen

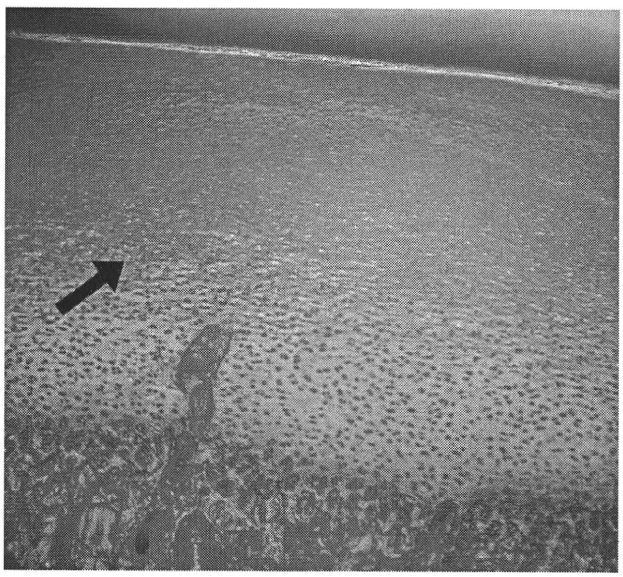

FIG. 3. Histological assessment of birefringence in 6-month-old porcine femoral cartilage specimens using polarized light microscopy. The cartilage samples were prepared as reported by Rieppo et al. (15) and Kiraly et al. (38). Decreased birefringence signal was shown in the superficial half of the cartilage (arrow).

fibers (19–22). On high-resolution T_2 maps of excised canine cartilage plugs, Xia et al. (19) found little orientation dependence of T_2 in the transitional zone, in contrast to the notable orientation dependence in the radial zone, with T_2 increasing by ~80% when the collagen fibers were aligned at 57° to B_0 compared with a 0° orientation. While evaluating the orientation effect on bulk cartilage T_2, Gründer et al. (22) observed the maximum increase in T_2 value when the radial zone was oriented at 55° to B_0, i.e., increasing by 300% compared with that at 0° orientation. To our knowledge, however, influence of the magic-angle effect on T_2 value has not been investigated with respect to the articular cartilage, using a more realistic joint model than the excised cartilage plugs.

In the present study, influence of the magic-angle effect on quantitative MR evaluation of the cartilage was investigated using en bloc knee joints retaining all intra-articular structures, the capsule, and the surrounding muscle. These animal knee joints were more realistic models than excised cartilage specimens. Intra-articular mechanical factors, which may have accelerating or competing effects on quantitative MR assessments in clinical MRI, cannot be investigated without using whole-knee models. Comparison of the MR assessments between positions A and C was aimed at evaluating the isolated influence of the magic-angle effect on the identical intra-articular biomechanical condition at an extended knee position. At position C, we expected that T_2 and T_2^* would increase at ROI 1 by changing the cartilage orientation more sensitive to the magic-angle effect and that those values would decrease at ROI 3 by changing the cartilage orientation less sensitive to the magic-angle effect. These expected tendencies were partly confirmed in our findings, with an increase of 6.8 and 11% at ROI 1 and a decrease of 12 and 6.7% at ROI 3 in T_2 and T_2^* values. However, the effect of orientation on cartilage was relatively small compared with that of previous findings using excised cartilage samples (19–22). With respect to dGEMRIC values, prior studies showed no orientational dependence of T_1 in the excised canine cartilage (19). The present findings also demonstrated a small change in the dGEMRIC value between positions A and C, with no significant difference.

MRI at knee flexion by 40° (position B) showed a more notable change in all examined parameters, resulting in a statistically significant difference in T_2 value at ROIs 1 and 3 and T_2^* value at ROI 1 and ROI 2. In comparison between positions A and B, the magnitudes of change at ROI 1 in T_2, T_2^*, and dGEMRIC values were more than three times greater than the changes observed in comparison between positions A and C. It is likely that factors other than the magic-angle effect also played an important role in the quantitative MR assessment changes associated with knee flexion. In the extended knee position, cartilage of ROI 1 is located in the weight-bearing portion of the femorotibial joint and is subject to relevant compressive and tensile force via interposed meniscus derived from preserved ligaments and the surrounding capsule. Cartilage of ROI 2 and ROI 3 is located in the non-weight-bearing portion of the femoral condyle and therefore is less subject to external compressed force. In the flexed knee position (position B), cartilage of ROI 1 was moved in the non-weight-bearing portion away from the meniscus, and the cartilage of ROI 3 was moved in the proximity of the patella-femoral joint. It is reasonable to consider that, according to knee flexion, the applied load-bearing force significantly decreased in the cartilage of ROI 1 and increased in the cartilage of ROI 3. Mesfar et al. (23) investigated the detailed biomechanics of knee joint during flexion movement by a three-dimensional computer-simulated technique and reported that tibiofemoral contact force was largest at full extension and decreased with joint flexion. Changes in the MR intensity and quantitative MR assessments in response to compressive loading were investigated thoroughly in experimental (9,24–26) and clinical studies (27–29). Rubenstein et al. (25) examined the MR appearance of an excised bovine cartilage under compressive force and observed a decrease in the signal intensity along the overall depth of the cartilage with a pressure of 1.10 MPa. In clinical MRI using a mechanical loading apparatus, significant decrease in the T_2 values was shown in the knee cartilage by loading 50–100% of the body weight during imaging (29,30). Decrease in the T_1 and T_2 values on loading has been accounted for by the deformation of cartilage architecture, extrusion of fluid content, and a relative increase in the proteoglycan and collagen content within the cartilage (25,27,28). Although changes in the pressure force on the cartilage were not directly measured in the present study, a significant increase in T_2 and T_2^* values at ROI 1 and decrease in T_2 values at ROI 3 by knee flexion were consistent with response to quantitative MR values due to the change in the biomechanical condition in the previous studies(23). In the present biochemical analysis, there was no difference of proteoglycan and hydroxyproline content among the three ROIs; however, T_2, T_2^*, and dGEMRIC values showed significant differences among the three ROIs. Although detailed zonal comparison along the cartilage depth was not conducted, lack of correlation between the quantitative MR values and the biochemical contents of the extracellular matrix may be partly accounted for by influence of localized biomechanical factors and/or the magic-angle effect. Mosher et al. (30) demonstrated a small difference in T_2 values between the cartilage zone orientated at 55° to B_0 and cartilage zone in parallel with B_0 in healthy volunteers and hypothesized that regional differences in the degree of cartilage compression are primarily responsible for the observed regional differences in the cartilage T_2. Our finding that T_2 measurement in the cartilage was influenced by both the magic-angle effect and localized biomechanical factors was in accordance with a previous clinical paper (30).

In the present study, we examined T_2, T_2^*, and dGEMRIC values as the major parameters in quantitative MR assessment of the cartilage. In prior ex vivo and in vivo studies, the T_2 value was assumed to be primarily correlated with water and collagen content or collagenous architecture (19,31), and the dGEMRIC value was assumed to be primarily sensitive to proteoglycan concentration within the cartilage (32). T_2^* assessment of the cartilage was studied in most recent investigations and assumed to be a potent alternative to T_2 assessment,

with faster scanning time (3). In spite of the assumed greater influence of the magic-angle effect on T_2 and T_2^* values than on T_1 value (17), the effect of orientational changes in the extended knee (position C) was similarly small in all three parameters. In knee flexion (position B), however, all three parameters showed a distinct increase at ROI 1, with the most pronounced change in T_2^* value. Although T_2 and T_2^* values were assumed to be sensitive to similar components of the cartilage and significant correlation between the two parameters was shown in our study, there may be considerable difference in sensitivity to the intracartilage component change and severity of other influential factors such as the magic-angle effect and susceptibility artifact around the bone–cartilage interface. Our results suggest that all three quantitative MR measurements may allow intra-articular biomechanical assessment in association with knee flexion. However, further studies are required to clarify the usefulness of individual MR parameters as a biomechanical surrogate.

Our study had several limitations. First, the small-diameter quadrature knee coil and gradient insert needed to perform the MR measurements did not allow the orientation of the femur to be varied by more than 40°. Therefore, MR measurements were not compared at two knee positions with a difference of the femoral shaft orientation around 55°, assuming it to present a maximum magic-angle effect. Change in the MR measurements of the articular cartilage at deep flexion, more than 40° in association with a different biomechanical condition of the intra-articular structures, was unknown. Second, the composition and thickness of the articular cartilage in different species may vary as a consequence of different load-bearing patterns, and the ex vivo whole-knee model did not incorporate surrounding muscle action such as contraction of the quadriceps or hamstrings or forces from surrounding ligamentous restraints. Severity and localization of change in the MR measurements, in association with knee flexion, may be different in human knee imaging in vivo. Third, although T_2, T_2^*, and dGEMRIC maps in this study were obtained with relatively high voxel resolution (voxel size 0.5 × 0.5 × 3.0 mm^3), the resolution is generally lower than that used in prior ex vivo studies. Because of the limited resolutions, assessment in layer-specific zones, such as superficial or deep layers of the cartilage, was not conducted in this study. The resultant volume-averaging effects might decrease the magnitude of the orientation effect. White et al. (33) assessed T_2 mapping characteristics of normal articular cartilage and of cartilage at sites of arthroscopic repair by in vivo imaging. Hannila et al. (34) assessed the topographical variation of T_2 relaxation time of articular cartilage in the young healthy knee joint. In these studies, MRI was performed using 1.5-T system and the voxel resolution was generally lower than in the present study. Juvenile porcine cartilage provided cartilage thickness similar to human adult cartilage. It is important to note that the resolution used in this study is similar to that used in high-resolution clinical imaging of the knee, and therefore our observations should be representative of the magnitude of the magic-angle effect that may be observed in routine clinical imaging. Fourth, previous histological investigations showed that immature pigs had less anisotropic collagen structure and different collagen fibril orientation with respect to the cartilage surface compared with matured pigs (15), and the 6-month-old porcine femoral cartilage in the present study was not matured yet. Using polarized light microscopy, however, we demonstrated that the 6-month-old porcine femoral cartilage had two zones with different anisotropy relating with collagen content and organization. Gründer et al. (9) showed the anisotropic zones determined by the arrangement of the collagenous network fibers of cartilage in juvenile animals. From our histological finding and those previous reports, we considered that the cartilage of juvenile pigs had certainly two zones with different anisotropy. Furthermore, it is important to clarify how T_2/T_2^*/dGEMRIC values in each layer would change at different positions; however, assessment in layer-specific zones was not conducted in this study due to the aforementioned limited resolution. The juvenile porcine cartilage might have less anisotropic collagenous structure and different collagen fibril orientation compared with mature porcine cartilage and human cartilage, and differences of magic-angle effect and change of quantitative MR assessments among examined species were unknown. Finally, we used freezing and thawing management in cadaver knees according to previous papers that reported freezing does not affect the material properties of cartilage (35,36). In contrast, Laouar et al. (37) showed that ice formation during cooling and warming of intact porcine articular cartilage caused a loss of fixed charged density throughout the articular cartilage matrix, reflecting changes in the content or structure of the proteoglycan component of the matrix. It is possible that freezing and thawing of cadaver knees affected collagen fiber orientation in cartilage, which is different from the clinical situation.

In conclusion, results of this study indicate that the effect of orientation on cartilage T_2 and T_2^* values in juvenile pigs is substantially less than that predicted on the basis of prior ex vivo studies. Substantial changes in T_2, T_2^*, and dGEMRIC values were demonstrated in response to knee flexion, presumably due to a change in the intra-articular biomechanical environment. After excluding the factor of the magic-angle effect, our results may suggest that quantitative MR measurements allow intra-articular biomechanical assessments in association with kinematic knee imaging.

ACKNOWLEDGMENTS

The authors thank Norinao Matsumoto and Yoshihiro Sakaguchi at the Matsumoto Medical Clinic and Yasuo Hara at the Department of Technology Development, IVTeC, Japan, for their technical assistance.

REFERENCES

1. Mosher TJ, Dardzinski BJ, Smith MB. Human articular cartilage: Influence of aging and early symptomatic degeneration on the spatial variation of T2-preliminary findings at 3 T. Radiology 2000;214: 259–266.
2. Dunn TC, Lu Y, Jin H, Ries MD, Majumdar S. T2 relaxation time of cartilage at MR imaging: comparison with severity of knee osteoarthritis. Radiology 2004;232:592–598.

3. Welsch GH, Mamisch TC, Hughes T, Zilkens C, Quirbach S, Scheffler K, Kraff O, Schweitzer ME, Szomolanyi P, Trattnig S. In vivo biochemical 7.0 tesla magnetic resonance: preliminary results of dGEMRIC, zonal T2, and T2* mapping of articular cartilage. Invest Radiol 2008;43:619–626.
4. Lammentausta E, Kiviranta P, Nissi MJ, Laasanen MS, Kiviranta I, Nieminen MT, Jurvelin JS. T_2 relaxation time and delayed gadolinium-enhanced MRI of cartilage (dGEMRIC) of human patellar cartilage at 1.5 T and 9.4 T: relationships with tissue mechanical properties. J Orthop Res 2006;24:366–374.
5. Burstein D, Velyvis J, Scott KT, Stock KW, Kim YJ, Jaramillo D, Boutin RD, Gray ML. Protocol issues for delayed $Gd(DTPA)^{2-}$-enhanced MRI (dGEMRIC) for clinical evaluation of articular cartilage. Magn Reson Med 2001;45:36–41.
6. Li X, Benjamin Ma C, Link TM, Castillo DD, Blumenkrantz G, Lozano J, Carballido-Gamio J, Ries M, Majumdar S. In vivo $T_{1\rho}$ and T_2 mapping of articular cartilage in osteoarthritis of the knee using 3T MRI. Osteoarthritis Cartilage 2007;15:789–797.
7. Scarvell JM, Smith PN, Refshauge KM, Galloway HR, Woods KR. Comparison of kinematic analysis by mapping tibiofemoral contact with movement of the femoral condylar centres in healthy and anterior cruciate ligament injured knees. J Orthop Res 2004;22:955–962.
8. Li G, Moses JM, Papannagari R, Pathare NP, DeFrate LE, Gill TJ. Anterior cruciate ligament deficiency alters the in vivo motion of the tibiofemoral cartilage contact points in both the anteroposterior and mediolateral directions. J Bone Joint Surg Am 2006;88:1826–1834.
9. Gründer W, Kanowski M, Wagner M, Werner A. Visualization of pressure distribution within loaded joint cartilage by application of angle-sensitive NMR microscopy. Magn Reson Med 2000;43:884–891.
10. Liess C, Lüsse S, Karger N, Heller M, Glüer CC. Detection of changes in cartilage water content using MRI T2-mapping in vivo. Osteoarthritis Cartilage 2002;10:907–913.
11. Mosher TJ, Smith HE, Collins C, Liu Y, Hancy J, Dardzinski BJ, Smith MB. Change in knee cartilage T2 at MR imaging after running: a feasibility study. Radiology 2005;234:245–249.
12. Rubenstein JD, Kim JK, Morova-Protzner I, Stanchev PL, Henkelman RM. Effects of collagen orientation on MR imaging characteristics of bovine articular cartilage. Radiology 1993;188:219–226.
13. Kurkijärvi JE, Nissi MJ, Rieppo J, Töyräs J, Kiviranta I, Nieminen MT, Jurvelin JS. The zonal architecture of human articular cartilage described by T2 relaxation time in the presence of $Gd\text{-}DTPA^{2-}$. Magn Reson Imaging 2008;26:602–608.
14. Nieminen MT, Rieppo J, Silvennoinen J, Töyräs J, Hakumäki JM, Hyttinen MM, Helminen J, Jurvelin JS. Spatial assessment of articular cartilage proteoglycans with Gd-DTPA-enhanced T1 imaging. Magn Reson Med 2002;48:640–648.
15. Rieppo J, Hyttinen MM, Halmesmaki E, Ruotsalainen H, Vasara A, Kiviranta I, Jurvelin JS, Helminen HJ. Changes in spatial collagen content and collagen network architecture in porcine articular cartilage during growth and maturation. Osteoarthritis Cartilage 2009;17:448–455.
16. Xia Y. Magic-angle effect in magnetic resonance imaging of articular cartilage: A review. Invest Radiol 2000;35:602–621.
17. Bydder M, Rahal A, Fullerton GD, Bydder GM. The magic angle effect: a source of artifact, determinant of image contrast, and technique for imaging. J Magn Reson Imaging 2007;25:290–300.
18. Peto S, Gillis P. Fiber-to-field angle dependence of proton nuclear magnetic relaxation in collagen. Magn Reson Imaging 1990;8:705–712.
19. Xia Y. Relaxation anisotropy in cartilage by NMR microscopy (muMRI) at 14-microm resolution. Magn Reson Med 1998;39:941–949.
20. Goodwin DW, Zhu H, Dunn JF. In vitro MR imaging of hyaline cartilage: correlation with scanning electron microscopy. AJR Am J Roentgenol 2000;174:405–409.
21. Mlynarik V, Degrassi A, Toffanin R, Vittur F, Cova M, Pozzi-Mucelli RS. Investigation of laminar appearance of articular cartilage by means of magnetic resonance microscopy. Magn Reson Imaging 1996;14:435–442.
22. Gründer W, Wagner M, Werner A. MR-microscopic visualization of anisotropic internal cartilage structures using the magic angle technique. Magn Reson Med 1998;39:376–382.
23. Mesfar W, Shirazi-Adl A. Computational biomechanics of knee joint in open kinetic chain extension exercises. Comp Methods Biomech Biomed Eng 2008;11:55–61.
24. Kaufman JH, Regatte RR, Bolinger L, Kneeland JB, Reddy R, Leigh JS. A novel approach to observing articular cartilage deformation in vitro via magnetic resonance imaging. J Magn Reson Imaging 1999;9:653–662.
25. Rubenstein JD, Kim JK, Henkelman RM. Effects of compression and recovery on bovine articular cartilage: appearance on MR images. Radiology 1996;201:843–850.
26. Wayne JS, Kraft KA, Shields KJ, Yin C, Owen JR, Disler DG. MR imaging of normal and matrix-depleted cartilage: correlation with biomechanical function and biochemical composition. Radiology 2003;228:493–499.
27. Liess C, Lüsse S, Karger N, Heller M, Glüer CC. Detection of changes in cartilage water content using MRI T_2-mapping in vivo. Osteoarthritis Cartilage 2002;10:907–913.
28. Nishii T, Kuroda K, Matsuoka Y, Sahara T, Yoshikawa H. Change in knee cartilage T_2 in response to mechanical loading. J Magn Reson Imaging 2008;28:175–180.
29. Nag D, Liney GP, Gillespie P, Sherman KP. Quantification of T_2 relaxation changes in articular cartilage with in situ mechanical loading of the knee. J Magn Reson Imaging 2004;19:317–322.
30. Mosher TJ, Smith H, Dardzinski BJ, Schmithorst VJ, Smith MB. MR imaging and T_2 mapping of femoral cartilage: in vivo determination of the magic angle effect. AJR Am J Roentgenol 2001;177:665–669.
31. Xia Y, Moody JB, Alhadlaq H. Orientational dependence of T_2 relaxation in articular cartilage: a microscopic MRI (microMRI) study. Magn Reson Med 2002;48:460–469.
32. Bashir A, Gray ML, Hartke J, Burstein D. Nondestructive imaging of human cartilage glycosaminoglycan concentration by MRI. Magn Reson Med 1999;41:857–865.
33. White LM, Sussman MS, Hurtig M, Probyn L, Tomlinson G, Kandel R. Cartilage T_2 assessment: differentiation of normal hyaline cartilage and reparative tissue after arthroscopic cartilage repair in equine subjects. Radiology 2006;241:407–414.
34. Hannila I, Räinä SS, Tervonen O, Ojala R, Nieminen MT. Topographical variation of T_2 relaxation time in the young adult knee cartilage at 1.5T. Osteoarthritis Cartilage 2009;17:1570–1575.
35. Kempson GE, Spivey CJ, Swanson SV, Freeman MR. Patterns of cartilage stiffness on normal and degenerate human femoral heads. J Biomech 1971;4:597–609.
36. Samosky JT, Burstein D, Grimson WE, Howe R, Martin S, Gray ML. Spatially-localized correlation of dGEMRIC-measured GAG distribution and mechanical stiffness in the human tibial plateau. J Orthop Res 2005;23:93–101.
37. Laouar L, Fishbein K, McGann LE, Horton WE, Spencer RG, Jomha NM. Cryopreservation of porcine articular cartilage: MRI and biochemical results after different freezing protocols. Cryobiology 2007;54:36–43.
38. Kiraly K, Hyttinen MM, Lapveteläinen T, Elo M, Kiviranta I, Dobai J, Modis L, Helminen HJ, Arokoski PA. Specimen preparation and quantification of collagen birefringence in unstained sections of articular cartilage using image analysis and polarizing light microscopy. Histochem J 1997;29:317–327.

Direct Anterior Cruciate Ligament Insertion to the Femur Assessed by Histology and 3-Dimensional Volume-Rendered Computed Tomography

Takehiko Iwahashi, M.D., Ph.D., Konsei Shino, M.D., Ph.D., Ken Nakata, M.D., Ph.D., Hidenori Otsubo, M.D., Tomoyuki Suzuki, M.D., Hiroshi Amano, M.D., and Norimasa Nakamura, M.D., Ph.D.

Purpose: The purpose of this study was to histologically identify the direct and indirect insertion of the femoral anterior cruciate ligament (ACL) insertion. Furthermore, we quantitatively measured the direct femoral insertion area by use of the 3-dimensional (3D) volume-rendered (VR) computed tomography (CT) model. **Methods:** By use of 8 intact cadaveric knees, the lateral femoral condyle including the ACL attachment was sectioned for histologic examination in 3 oblique-axial planes parallel to the roof of the intercondylar notch and in the sagittal planes. Before sectioning, these knees had been subjected to CT to obtain 3D VR images of the femur. Once the direct insertion of the ACL was identified on each histologic section, the corresponding image was superimposed on the corresponding CT image. **Results:** The direct ACL insertion, in which dense collagen fibers were connected to the bone by the fibrocartilaginous layer, was microscopically identified at the region between the posteromedial articular cartilage margin of the lateral femoral condyle and the linear bony ridge 7 to 10 mm anterior to the articular cartilage margin. Meticulous comparison of histologic analysis and the 3D VR CT model showed that the ACL direct insertion coincided with a crescent-shaped hollow just behind the linear bony ridge. The direct insertion measured 17.4 ± 0.9 mm (mean ± SD) in length, 8.0 ± 0.5 mm in width, and 128.3 ± 10.5 mm^2 in area. **Conclusions:** The direct insertion of the ACL is located in the depression between the resident's ridge and the articular cartilage margin on the lateral femoral condyle. It measured 17.4 ± 0.9 mm in length, 8.0 ± 0.5 mm in width, and 128.3 ± 10.5 mm^2 in area. **Clinical Relevance:** Delineation of the ACL femoral direct insertion by 3D VR CT could be a useful tool for planning of accurate femoral tunnel positioning in anatomic ACL reconstruction.

Ligaments are discrete bands of dense connective tissue that span joints and connect bones and thus serve an important role in both stabilizing joints and guiding joint motion. Ligaments have 2 unique modes of insertion to the bone, namely direct insertion and indirect insertion. Direct insertion has a zonal architecture including the transition from ligamentous tissue, noncalcified cartilage, and calcified cartilage to bone, which allows for a gradual force distribution and differential tensioning of all inserting components into the insertion site.[1,2] The indirect type of insertion has a significantly simpler ultrastructure, where the ligament directly anchors to the bone by collagen fibers without forming a clear transitional zone. These fibers represent the equivalent to the collagen fibers anchoring the periosteum to bone as described by Benjamin.[3] The direct insertion type represents a firm and fixed attachment allowing for a gradual load distribution into the subchon-

From the Department of Orthopaedics (T.I., K.N., H.A., N.N.), Osaka University Graduate School of Medicine, Osaka; Faculty of Comprehensive Rehabilitation (K.S.), Osaka Prefecture University, Osaka; and Department of Orthopaedics (H.O., T.S.), Sapporo Medical University, Sapporo, Japan.

The authors report no conflict of interest.

Received November 19, 2008; accepted January 26, 2010.

Address correspondence and reprint requests to Takehiko Iwahashi, M.D., Ph.D., Department of Orthopaedics, Osaka University Graduate School of Medicine, 2-2 Yamadaoka, Suita, Osaka 565-0871, Japan. E-mail: tiwa1884@yahoo.co.jp

0749-8063/8659/$36.00

doi:10.1016/j.arthro.2010.01.023

dral bone and, from a biomechanical point of view, is thus extremely important as a key link between the ligament and bone to transmit mechanical load to the joint.[4]

Several studies have reported on the anterior cruciate ligament (ACL) femoral attachment area by macroscopic observation[5-14]; however, such studies only identified the overall profile of the femoral attachment area of the ACL. In contrast, there have been a limited number of studies that microscopically analyzed the femoral insertion of the ACL, and no study has specifically identified the area of the direct femoral insertion of the ACL. Ferretti et al.[6] performed a histologic examination of the ACL femoral footprint, but they only referred to the lateral bifurcate ridge without evaluation of the insertion site.

Ferretti et al.[6] also quantitatively showed the landmarks of the femoral attachment of the ACL by 3-dimensional (3D) modeling using a 3D laser digitizer. Because 3D images obtained by the 3D laser digitizer theoretically delineate the traced surface figure,[15] the 3D modeling of the femoral attachment in their study might not have accurately delineated the bony surface because of potential contamination of surface soft tissue. In this regard, it is known that 3D volume-rendered (VR) computed tomography (CT) can accurately delineate the surface of any bony structure.[16,17]

The purposes of our study were to histologically identify the direct and indirect insertion of the femoral ACL attachment area and to quantify the direct insertion area by superimposing the microscopic anatomy of the region onto the 3D VR CT model of the femoral condyle.

The hypotheses of this study were that (1) there may be a direct insertion type microscopically identified inside the ACL femoral attachment area and (2) the direct insertion area may be delineated by a bony surface landmark.

METHODS

We obtained 8 ACL-intact knees (4 paired knees) from 4 embalmed cadavers (3 men and 1 woman aged between 66 and 87 years, with a mean age of 77 years) with a height of 151 to 170 cm (mean ± SD, 162 ± 8.0 cm) for this study. The cadavers were fixed in 8% formalin and preserved in 30% ethanol. The muscle around the knee joint, as well as the capsular ligament with patella, was removed to allow thorough examination of the interior of the joint. The posterior cruciate ligament was also removed. Then, the ACL was detached from the tibial attachment.

The femur was cut at 15 cm from the joint surface and was longitudinally split with an oscillating saw in the sagittal plane, including the highest point of the anterior outlet of the intercondylar notch.

Macroscopic Observation of ACL Femoral Footprint

The ACL femoral footprint was macroscopically analyzed to determine the extent of ligament fiber distribution by pulling the ACL in the anteroinferior or posterosuperior direction parallel to the roof of the notch.

CT Scanning and Image Reconstruction

CT scans of the femur were taken under the conditions of 120 kV, 100 mA, and a 1-mm slice thickness (ProSpeed AI system; GE Healthcare, Waukesha, WI).

The CT data were processed with software for image analysis (Virtual Place-M; AZE, Tokyo, Japan), and the femoral contour was automatically extracted from the images (segmentation). A 3D bone surface model was constructed by the marching cube technique. The images were made up of numerous tiny triangles, each of which contained the positional data for 3 points. Reconstructed images were viewed by use of a modified version of Visualization Tool Kit (VTK) software (Kitware, Clifton Park, NY). Specifically, CT images of the lateral femoral condyle along the oblique-axial planes parallel to the roof of the notch, identical to the sections for histologic analysis (slices 1, 2, and 3), were made (Fig 1A). A plane parallel to the medial aspect of the lateral femoral condyle was also generated (Fig 1B).

Histologic Examination of ACL Attachment Area to Femur

All 8 lateral femoral condyles, with preservation of the ACL femoral footprint, were decalcified in hydrochloric acid and embedded in paraffin for light microscopy. We cut 4 specimens from the 4 cadavers into 3 blocks of even thickness along the oblique-axial planes parallel to the roof of the notch, and their sections were sliced into 5-μm specimens, stained with H&E, and observed under a microscope (Nikon ECLIPSE 90i; Nikon, Melville, NY) at a magnification of ×40 to meticulously indentify the attachment area including the insertion of dense collagen fibers and surrounding coarse fibrous tissues (Fig 1A, slices 1, 2, and 3). For quantification of the insertion area, the anteroposterior distance on the medial aspect of the lateral femoral condyle in slices 1, 2, and 3 was measured with a slide caliper under a microscope.

The remaining 4 specimens were cut at the level of the attachment area along the sagittal plane, sliced into

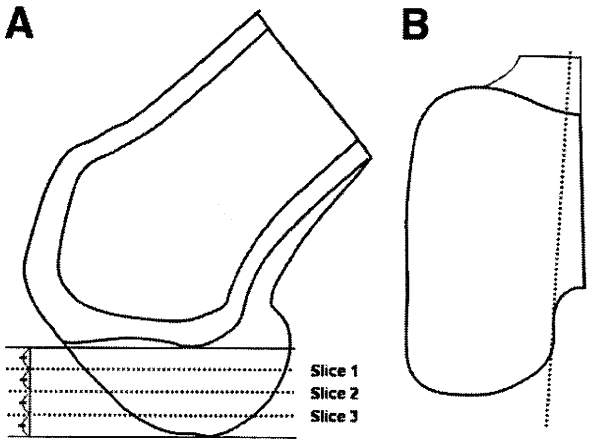

FIGURE 1. Demographic description of section planes for histologic analysis. (A) The lateral femoral condyle is cut into 4 blocks at even intervals along the oblique-axial planes parallel to the roof of the notch, and the superior-anterior section (slice 1), middle section (slice 2), and inferior-posterior section (slice 3) are subjected to histologic analysis. (B) The lateral femoral condyle is cut at the level of the attachment area along the sagittal plane to perpendicularly determine the ligament attachment area.

5-μm specimens, stained with hematoxylin, and observed under a light microscope (Fig 1B). Histologic analysis was performed by 3 orthopaedic surgeons (T.I., H.O., and T.S.).

Superimposition of CT Images on Histologic Data

Comparison of Histologic Preparations and Slices From 3D VR CT Model: Each of the histologic slices (slices 1, 2, and 3) was compared with the corresponding CT images to assess the bony surface morphology around the direct insertion of the ACL. First, the area of direct insertion of the ACL on the lateral femoral condyle was measured on microscopic histologic images of slices 1, 2, and 3 with slide calipers. Then, the histologic image of each slice was superimposed on the CT model image of the corresponding slice to project the ACL femoral attachment area. The dimensions of the attachment area were measured on the reconstructed slices from the 3D VR CT model.

Evaluation of Position and Area of Direct Insertion of ACL by 3D VR CT Model: On the basis of the microscopic data, the region of the direct insertion of the ACL was superimposed on the slices from the 3D VR CT model. The area of the direct insertion of the ACL was calculated on the 3D VR CT model by use of computer software (Kitware).

RESULTS

Macroscopic Observation of ACL Femoral Attachment Area and Bony Surface Around Area

The ACL fibers ran anteriorly-inferiorly, parallel to the roof of the intercondylar notch (Fig 2A). Obviously, the attachments were located in the posterior-superior quarter of the lateral wall of the notch. Although the whole attachment area was apparently broad with an oval shape (Fig 2B), when the dense fiber of the ACL substance (Fig 2E) was inverted posteriorly-superiorly to observe the anterior border of its attachment area, it was found that the border formed a linear line demarcating the posterior-superior quarter of the lateral wall of the notch, extending to a line comprising the posterior cortical border of the femoral diaphysis (Fig 2B). The posterior surface of the ACL attachment area extended to the cartilage margin of the lateral femoral condyle (Fig 2C). The dense fibrous tissue of the ACL inserted into the concave area (Fig 2D) located in the very distant portion of the lateral wall of the notch.

Microscopic Findings of ACL Attachment Area to Femur

Observation from either the oblique axial planes parallel to the roof of the notch (Fig 3A) or sagittal planes (Fig 3B) showed that the linear bony ridge formed the anterior-inferior rim of the dense collagen fiber attachment of the ACL (Fig 3A, large arrow). The femoral attachment area extended posteriorly and superiorly to the articular cartilage margin (Fig 3A, small arrows). Observation by the oblique axial planes parallel to the roof of the notch enabled the delineation of the central dense collagen fibers (Fig 3A, oval) from the attachment of the surrounding coarse fibrous tissues. The dense collagen fibers directly inserted into the concave area (Fig 3A, arrowheads) behind the bony ridge (Fig 3A, large arrow), whereas coarse fibrous tissues attached to the bone just anterior to the bony ridge or the concavity. A higher-magnification view showed that the attachment area of the coarse fibrous tissue surrounded the dense fiber attachment area extending anteriorly over the bony ridge (Fig 3C). It also showed that the dense fibers attached to the bone by direct insertion with the zonal transition from ligamentous tissue, noncalcified cartilage, and calcified cartilage to bone (Figs 3D, 3G, and 3H).

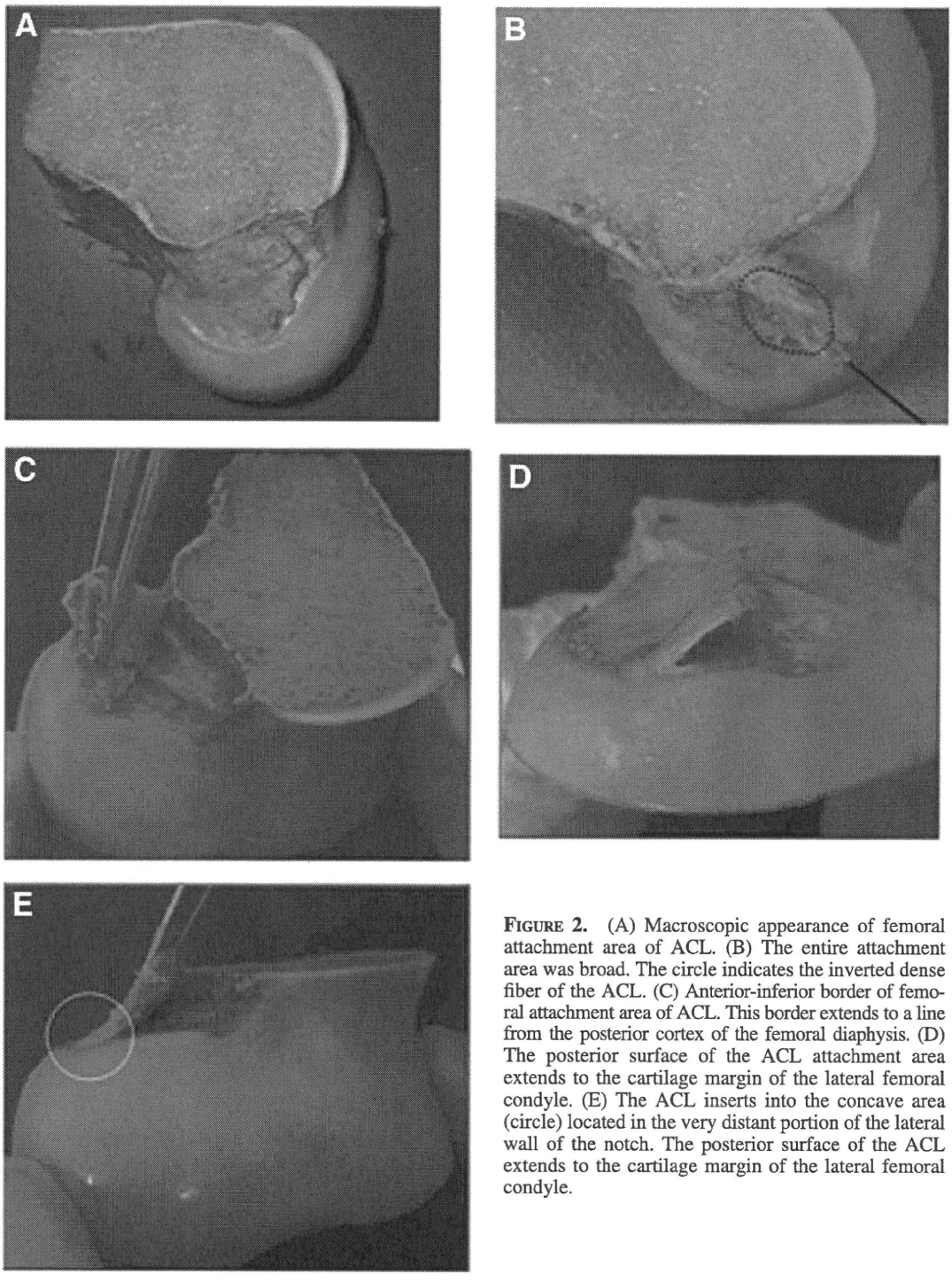

FIGURE 2. (A) Macroscopic appearance of femoral attachment area of ACL. (B) The entire attachment area was broad. The circle indicates the inverted dense fiber of the ACL. (C) Anterior-inferior border of femoral attachment area of ACL. This border extends to a line from the posterior cortex of the femoral diaphysis. (D) The posterior surface of the ACL attachment area extends to the cartilage margin of the lateral femoral condyle. (E) The ACL inserts into the concave area (circle) located in the very distant portion of the lateral wall of the notch. The posterior surface of the ACL extends to the cartilage margin of the lateral femoral condyle.

On the other hand, in the region adjacent to the direct insertion area, the coarse fibrous tissues attached to the bone through indirect insertion without the cartilaginous transition zones (Figs 3C, 3E, 3F, and 3I).

Quantitative Evaluation of Direct Insertion of ACL by Histology and 3D VR CT

Comparison of Histology With CT Image: On both the histologic images and the 3D VR CT images, an elevated bony ridge was observed in the anterior

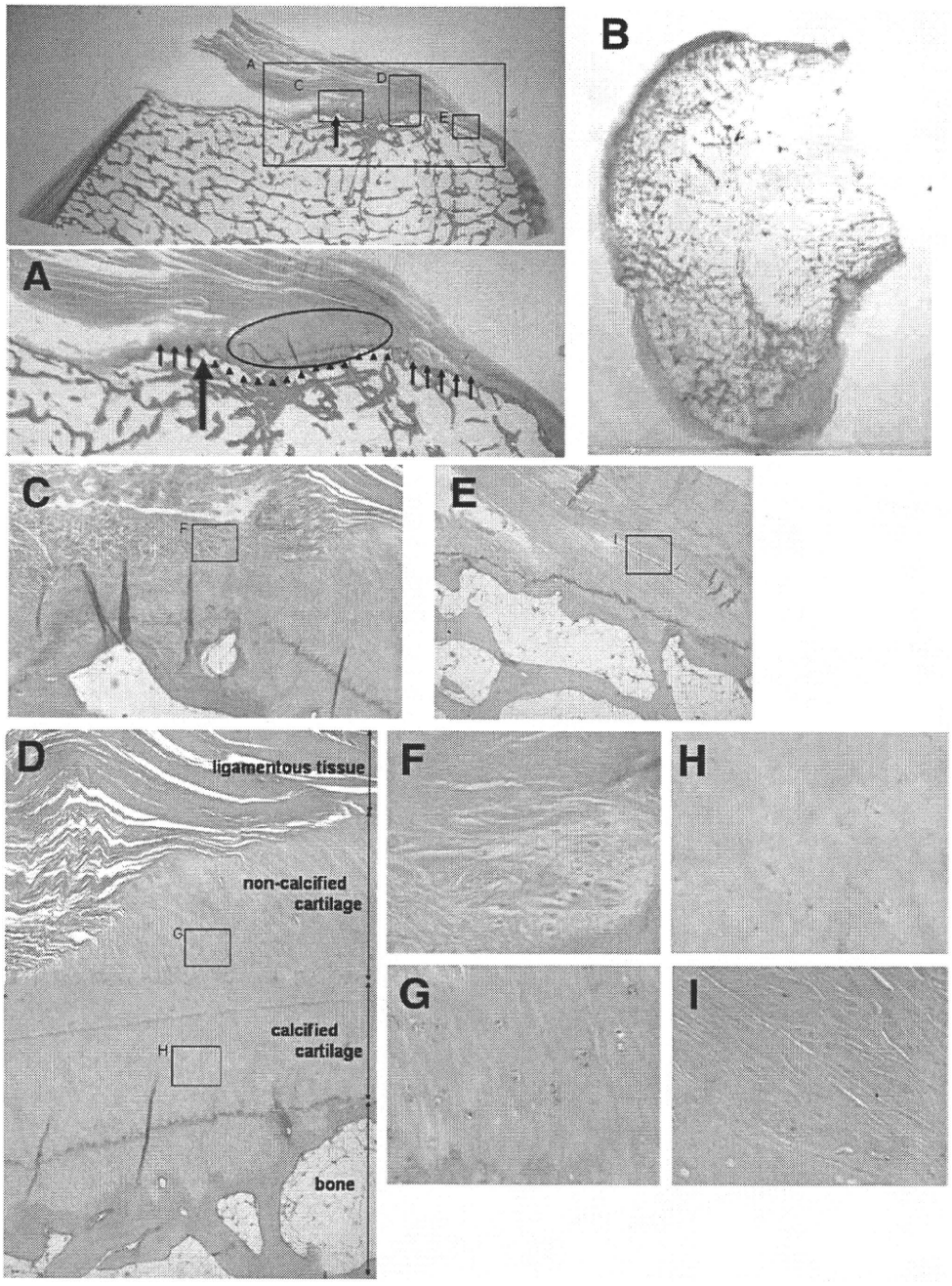

FIGURE 3. Histology of ACL attachment area to lateral femoral condyle (H&E stain). (A) Section from oblique axial plane parallel to roof of notch (original magnification ×5). The presence of bony prominence is confirmed (large arrow) adjacent to the anterior border of the concave area (arrowheads), and central dense collagenous fibers (oval) insert into the concave area behind the bony ridge. The coarse fibrous region is surrounded by the central dense collagenous fibers and attached to the bone around the bony ridge and the concavity (small arrows). The coarse fibrous region extended posteriorly in contact with the margin of the articular cartilage. (B) Schematic diagram of direct insertion area of ACL attachment area on lateral femoral condyle (sagittal plane through medial part of lateral condyle) (original magnification ×5). (C) Higher-magnification view of attachment area of coarse fibrous region around bony ridge (original magnification ×40). There are no cartilaginous transition zones, and the indirect insertion is developed. (D) Higher-magnification view of attachment area of central dense collagenous fibers to bone (original magnification ×40). (E) Higher-magnification view of coarse fibrous region extending posteriorly in contact with margin of articular cartilage (original magnification ×40). (F) Higher-magnification view of attachment area of coarse fibrous region around bony ridge (original magnification ×400). There are no cartilaginous transition zones, and the indirect insertion is developed. (G) Higher-magnification view of noncalcified cartilage in direct insertion (original magnification ×400). (H) Higher-magnification view of calcified cartilage in direct insertion (original magnification ×400). The direct insertion, which represented the transition from ligamentous tissue, noncalcified cartilage, and calcified cartilage to bone, is conformed. (I) Higher-magnification view of attachment area of coarse fibrous region extending posteriorly in contact with margin of articular cartilage (original magnification ×400). There are no cartilaginous transition zones, and the indirect insertion is developed.

margin of the direct insertion of the ACL. The 3D VR CT model reproduced the characteristic bony surface morphology of the concave area that extended from the bony elevation to the posterior margin of the medial aspect of the lateral femoral condyle (Fig 4). Notably, close comparison of the histology with the CT images showed that the concave area in the medial aspect of the lateral femoral condyle on the CT images corresponded with the region of direct insertion of the ACL observed in the histologic sections. The anteroposterior width of the concave area was calculated as 7.9 ± 0.9 mm (mean ± SD) by CT and 7.8 ± 1.0 mm by histology at the slice 1 level. The width was calculated as 9.6 ± 0.7 mm by CT and 9.5 ± 0.6 mm by histology at the slice 2 level and 8.9 ± 0.8 mm by CT and 8.6 ± 0.5 mm by histology at the slice 3 level (Fig 5). The results are summarized in Table 1. With regard to the reliability of measurements made by CT and histology, the SDs and coefficients of variation for intraobserver and interobserver variability are shown in Table 2.

Location and Area of Collagenous ACL Fiber Insertion on 3D VR CT Images: The concavity observed on the 3D VR CT images was 17.4 ± 0.9 mm (mean ± SD) in length, 8.0 ± 0.5 mm in width, and 128.3 ± 10.5 mm^2 in area (Fig 4). The other measured data are listed in Table 3.

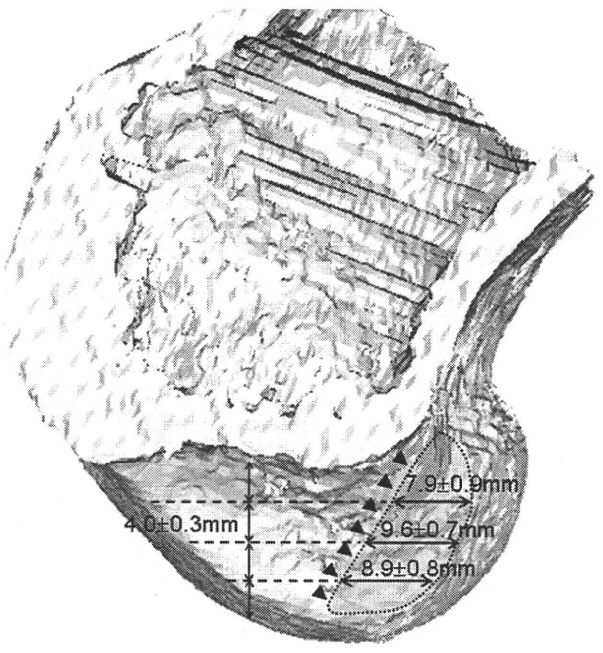

FIGURE 4. Three-dimensional VR CT model of lateral femoral condyle. The resident's ridge (arrowheads) is located proximal-distal along the entire ACL attachment.

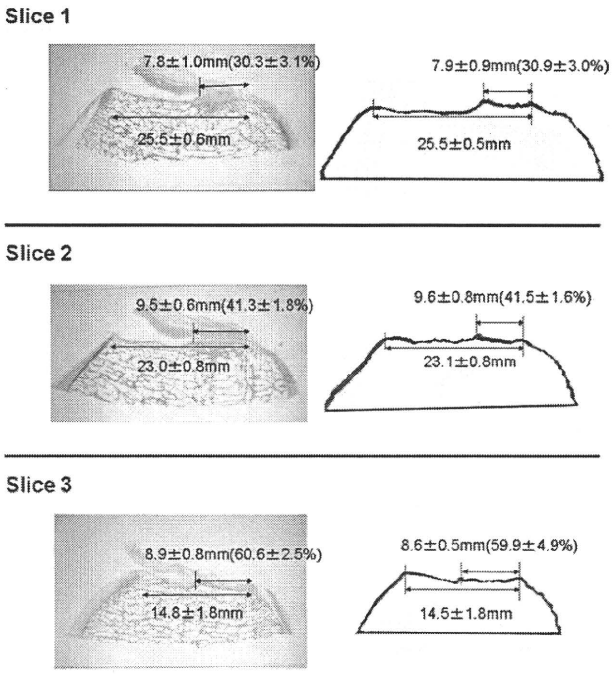

FIGURE 5. Semi-quantification of area of ACL attachment area on lateral femoral condyle by oblique axial planes parallel to roof of notch (corresponding to slices 1, 2, and 3 in Fig 1A). The ACL attachment area occupies 30.3% ± 3.1% (mean ± SD) in the superior-anterior sections, 41.3% ± 1.8% in the middle sections, and 60.6% ± 2.5% in the inferior-posterior sections. H&E stain, original magnification ×0.7.

DISCUSSION

Although the concept of anatomic reconstruction has been a trend in ACL reconstruction,[5,18] the definition of the term "anatomic" is not yet well defined. This may be mainly because of inconsistency in the definition of the geographic location of the ACL in-

TABLE 1. *Quantitative Evaluation of Region for Direct Insertion of ACL by Histology and Region of Depressed Area on 3D VR CT Model*

	Histology		CT Model	
	Mean	Range	Mean	Range
Length of lateral femoral condyle (mm)				
Slice 1	25.5 ± 0.6	25-26	25.5 ± 0.5	24.9-26.1
Slice 2	23.0 ± 0.8	22-24	23.1 ± 0.8	22.3-24.1
Slice 3	14.5 ± 1.7	13-17	14.8 ± 1.8	12.9-17.1
Footprint length (mm)				
Slice 1	7.8 ± 1.0	7-9	7.9 ± 0.9	7.1-8.8
Slice 2	9.5 ± 0.6	9-10	9.6 ± 0.7	8.8-10.3
Slice 3	8.6 ± 0.5	8-10	8.9 ± 0.8	7.9-9.7

TABLE 2. *Intraobserver and Interobserver SDs and Coefficients of Variation for 6 Parameters on Histologic or CT Evaluation*

	Histology				CT Model			
	Intraobserver		Interobserver		Intraobserver		Interobserver	
	SD (mm)	CV (%)	SD (mm)	CV (%)	SD (mm)	CV (%)	SD (mm)	CV (%)
Length of lateral femoral condyle								
Slice 1	0.6	2.3	0.6	2.3	0.5	2.1	0.5	2.1
Slice 2	0.0	0.0	0.6	2.4	0.3	1.3	0.6	2.3
Slice 3	0.6	3.3	0.0	0.0	0.6	3.5	0.4	2.1
Footprint length								
Slice 1	0.0	0.0	0.6	6.2	0.3	1.2	0.4	4.1
Slice 2	0.6	5.6	0.0	0.0	0.6	3.6	0.4	2.4
Slice 3	0.6	6.2	0.0	0.0	0.5	4.2	0.3	1.3

Abbreviations: CV, coefficient of variation.

sertion to the lateral femoral condyle.[5-14] In this study we have identified that the ACL insertion consists of 2 different structures, the direct insertion and the indirect insertion, by histologic analysis. Previous studies suggested that the direct insertion plays a major role in the mechanical link between the ligament and bone as compared with the indirect insertion,[1,2,7] and therefore, in anatomic ACL reconstruction, it may be reasonable to create the femoral tunnels within the direct insertion area. However, by macroscopic observation, it was impossible to distinguish the direct and indirect insertions. If one takes into account that most previous studies to identify the femoral footprint of the ACL have been done by macroscopic observation,[5-14] there is the potential risk of dismissing the relative ratio of functional importance between the direct and indirect insertions within the ACL footprint, which might be misleading with regard to the recommended geographic location of the femoral bone tunnels at the time of anatomic ACL reconstruction.

Notably, the bony surface of the direct insertion showed a concavity, and there was a prominence of the bony ridge adjacent to the anterior border of this concavity. This bony ridge geographically coincides with the "resident's ridge" proposed by Clancy and colleagues.[17] Hutchinson and Ash[19] also reported the existence of the resident's ridge at the anterior rim of the ACL attachment site, based on the results of microscopic investigation. Our macroscopic and microscopic observations showed that the ridge described by Hutchinson and Ash corresponds to the osseous elevation that was detected adjacent to the anterior border of the ACL direct insertion.

TABLE 3. *Two-Dimensional Measurements of ACL Direct Insertion*

	Mean	Range
Footprint length (mm)	17.4 ± 0.9	16.2-18.4
Footprint width (mm)	8.0 ± 0.5	7.1-8.3
Length of resident's ridge (mm)	14.5 ± 0.9	13.2-15.3
Height of resident's ridge (mm)	0.8 ± 0.1	0.7-0.9
Footprint area (mm^2)	128.3 ± 10.5	113.6-137.5

Previous reports on the location of the ACL attachment, including those of Colombet et al.[10] and Amis and Jakob,[8] indicated that the ACL attached to the lateral condyle of the femur at a site posterior to a line extending from the posterior cortex of the femoral diaphysis. Girgis et al.[11] reported that the ACL attachment area on the lateral femoral condyle was semicircular with a posterior bulge and a linear anterior rim. A more recent study by Purnell et al.[17] using high-resolution VR CT showed the relation between the ACL femoral attachment and the resident's ridge, as well as its location. The location of the ACL attachment and the resident's ridge reported in their study was exactly identical to that of the direct ACL insertion area presented in our study.

Ferretti et al.[6] also quantitatively reported on the 3D landmarks of the femoral attachment of the ACL using a 3D laser digitizer. The 3D laser digitizer theoretically traces the surface geometry of the specimen of interest and could potentially include the surface soft-tissue structures, and thus the image does not represent the bony surface landscape.[15] In fact, the area of ACL attachment area reported by Ferretti et al. was 196 mm^2, much larger than that observed in our study

(128 mm^2). If one takes into account that our 3D VR CT image accurately represents the bony surface landscape, such discrepancy might be attributed to the inclusion of the surface soft tissues in their study.[6] Furthermore, in terms of clinical implications, 3D VR CT has the advantage over the 3D laser digitizer, in that 3D VR CT can be applied to every patient clinically without an invasive procedure, and thus the 3D evaluation of the bony landmark to identify the ACL direct insertion can serve as a very useful tool for preoperative planning.

The limitation of this study was that we did not specifically observe the insertion of the separate bundles (anteromedial or posterolateral). However, the information about the location of the direct insertion of the ACL, which plays a pivotal biomechanical function, could be beneficial to the performance of anatomic and functional ACL reconstruction surgery. For anatomic reconstruction of the ACL, it is recommended to create a bone tunnel within the area we described by 3D VR CT as the direct attachment area or insertion in Fig 5. We believe that the bony surface landmark identified in this study could be helpful in all "anatomic" ACL reconstruction procedures regardless of the number of femoral tunnels (single or double) or the choice of graft materials.

CONCLUSIONS

The direct insertion of the ACL is located in the depression between the resident's ridge and the articular cartilage margin on the lateral femoral condyle. It measured 17.4 ± 0.9 mm in length, 8.0 ± 0.5 mm in width, and 128.3 ± 10.5 mm^2 in area.

REFERENCES

1. Schneider H. Structure of tendon attachments. *Z Anat Entwicklungsgesch* 1956;119:431-456 (in German).
2. Weiler A, Scheffler S. Healing of ligament and tendon to bone. In: Walsh WR, ed. *Orthopedic biology and medicine: Repair and regeneration of ligaments, tendons, and joint capsule.* Totowa, NJ, Humana Press, 2005;201-231.
3. Benjamin M, Evans EJ, Copp L. The histology of tendon attachment to bone in man. *J Anat* 1986;149:89-100.
4. Benjamin M, Moriggl B, Brenner E, Emery P, McGonagle D, Redman S. The "enthesis organ" concept: Why enthesopathies may not present as focal insertional disorders. *Arthritis Rheum* 2004;50:3306-3313.
5. Yasuda K, Kondo E, Ichiyama H, et al. Anatomic reconstruction of the anteromedial and posterolateral bundles of the anterior cruciate ligament using hamstring tendon grafts. *Arthroscopy* 2006;20:1015-1025.
6. Ferretti M, Ekdahl M, Shen W, Fu FH. Osseous landmarks of the femoral attachment of the anterior cruciate ligament: An anatomic study. *Arthroscopy* 2007;23:1218-1225.
7. Takahashi M, Doi M, Abe M, Suzuki D, Nagano A. Anatomical study of the femoral and tibial insertions of the anteromedial and posterolateral bundles of human anterior cruciate ligament. *Am J Sports Med* 2006;34:787-792.
8. Amis AA, Jakob RP. Anterior cruciate ligament graft positioning, tensioning and twisting. *Knee Surg Sports Traumatol Arthrosc* 1998;6:S2-S12 (Suppl 1).
9. Bernard M, Hornung H, Cierpinski T. Femoral insertion of the ACL. Radiographic quadrant method. *Am J Knee Surg* 1997; 10:14-22.
10. Colombet P, Robinson J, Christel P, et al. Morphology of anterior cruciate ligament attachments for anatomic reconstruction: A cadaveric dissection and radiographic study. *Arthroscopy* 2006;22:984-992.
11. Girgis FG, Marshall JL, Monajem A. The cruciate ligaments of the knee joint. Anatomical, functional and experimental analysis. *Clin Orthop Relat Res* 1975:216-231.
12. Giron F, Cuomo P, Aglietti P, Bull AM, Amis AA. Femoral attachment of the anterior cruciate ligament. *Knee Surg Sports Traumatol Arthrosc* 2006;14:250-256.
13. Harner CD, Baek GH, Vogrin TM, Carlin GJ, Kashiwaguchi S, Woo SL. Quantitative analysis of human cruciate ligament insertions. *Arthroscopy* 1999;15:741-749.
14. Mochizuki T, Muneta T, Nagase T, Shirasawa S, Akita KI, Sekiya I. Cadaveric knee observation study for describing anatomic femoral tunnel placement for two-bundle anterior cruciate ligament reconstruction. *Arthroscopy* 2006;22:356-361.
15. Keating AP, Knox J, Bibb R, Zhurov AI. A comparison of plaster, digital and reconstructed study model accuracy. *J Orthod* 2008;35:191-201.
16. Moritomo H, Goto A, Sato Y, Sugamoto K, Murase T, Yoshikawa H. The triquetrum-hamate joint: An anatomic and in vivo three-dimensional kinematic study. *J Hand Surg Am* 2003;28:797-805.
17. Purnell ML, Larson AI, Clancy W. Anterior cruciate ligament insertions on the tibia and femur and their relationships to critical bony landmarks using high-resolution volume-rendering computed tomography. *Am J Sports Med* 2008;36:2083-2090.
18. Shino K, Nakata K, Nakamura N, et al. Anatomic anterior cruciate ligament reconstruction using two double-looped hamstring tendon grafts via twin femoral and triple tibial tunnels. *Oper Tech Orthop* 2005;15:130-134.
19. Hutchinson MR, Ash SA. Resident's ridge: Assessing the cortical thickness of the lateral wall and roof of the intercondylar notch. *Arthroscopy* 2003;19:931-935.

内側半月板水平断裂の膝屈伸における変位・変形のMRI 3次元動態解析

天野　大[※1]　中田　研[※2]　岩橋　武彦[※2]　鈴木　智之[※3]
前　達雄[※2]　中村　憲正[※2]　菅本　一臣[※4]　吉川　秀樹[※2]
史野　根生[※5]

In vivo 3-D Dynamic MRI Evaluation of Movement, Deformation of Meniscus with Horizontal Tear.

Hiroshi AMANO, MD., Ken NAKATA, MD. PhD., Takehiko IWAHASHI, MD. PhD., Tomoyuki SUZUKI, MD., Tatsuo MAE, MD. PhD., Norimasa NAKAMURA, MD. PhD., Kazuomi SUGAMOTO, MD. PhD., Hideki YOSHIKAWA, MD. PhD., Konsei SHINO, MD. PhD.

Abstract

This study quantitatively evaluated the three-dimensional deformation and movement of the horizontally-torn menisci during knee flexion.

Nine knees with horizontally-torn medial menisci were analyzed using 3-D MRI from 0 to 60 degrees of flexion in 20-degree increments. Serial images were segmented to produce 3-D models of each knee angle. After matching each 3-D models of tibia using the volume-based registration method, three-dimensional deformation and movement of the meniscus during knee flexion were visualized and quantitatively evaluated.

Four of nine torn menisci with tear sizes in the horizontal plane exceeding more than 40% of the circumferential length showed different deformation patterns than those of normal menisci and their gaps opened by more than 2 mm with flexion. Other tears measuring less than 30% of the circumferential length opened by no more than 2 mm and showed movement and deformation patterns similar to those of normal menisci during flexion.

Horizontal tear more than 40% in circumferential length showed paradoxical movement and deformation, and opened by more than 2 mm with knee flexion.

Key words : 3-D MRI, Movement and deformation of meniscus, medial meniscus with horizontal tear.

※ 1　市立豊中病院　整形外科
〒560-8565　大阪府豊中市柴原町4-14-1

※ 2　大阪大学大学院　医学系研究科器官制御外科
〒565-0871　吹田市山田丘2-2
※ 3　札幌医科大学　整形外科
〒060-8556　札幌市中央区南１条西17丁目
※ 4　大阪大学大学院　医学系研究科運動器バイオマテリアル学
〒565-0871　吹田市山田丘2-2
※ 5　大阪府立大学　総合リハビリテーション学部
〒583-8555　羽曳野市はびきの3-7-30

Corresponding Author : Hiroshi AMANO, MD.
Department of Orthopaedic Surgery Toyonaka Municipal Hospital
4-14-1, Shibahara-cho, Toyonaka, Osaka 560-0055, Japan
Tel : +81-6-6843-0101　Fax : +81-6-6858-3531
E-mail address : h-amano@umin.ac.jp

はじめに

半月板の機能については，1948年にFairbankらが半月板の荷重分散機能について報告[6]して以来，関節安定性や関節潤滑，衝撃吸収，関節固有感覚への関与などが報告されている[1),11)]．膝屈伸時には，大腿骨と脛骨の動きに合わせて半月板が動くことで関節適合性が維持され，膝屈伸時にもこれらの機能をはたすことができている[8),10),12)]．

近年，MRIを用いた正常半月板の動態解析の報告がされている．Thompsonらは屍膝を用いて，膝屈曲に伴い半月板は後方へ移動し，内側半月板に比べ外側半月板が大きく動くと報告している[13)]．またVediらは生体膝を垂直型のopen MRIにて撮影し，立位荷重時には非荷重時に比べて半月板の移動量が大きくなることを報告している[15)]．

一方で，Boxheimerらは損傷半月板の動態解析について，垂直型openMRIを用いて報告している[3)]．その中で，環状断面では縦断裂と横断裂，complex tearで膝屈曲と回旋を加えたときに半月板が外側にdisplaceし，水平断裂ではあまりdisplaceしなかったと述べている．しかし，水平断裂は後節から後角に損傷の多く，膝屈伸による変位，変形は環状断面よりも矢状断面のほうが観察できると考えられるが，水平断裂を伴った半月板の動態を矢状断面で詳細に検討している報告はない．

そこで我々は，症状のある内側半月板水平断裂の膝関節屈伸に伴う変位・変形と損傷部の大きさを，３次元（3-dimentional，3-D）MRIと3-Dコンピューターモデルを用いて定量評価し，病態について検討した．

対　　象

内側半月板にMRIで水平断裂（Mink grade 3）を認め，半月板由来と考えられる症状を有し，水平断裂以外の損傷形態がなく，半月板以外の膝関節内および膝周囲に異常がない症例を対象とした．これらの条件に合致した９名９膝であった．男６例女３例で，平均年齢39.7歳（17～50歳）であった．

全例に本研究についての説明を十分に行いinformed consentを得た．

方　　法

１．MRI撮影

MRIの撮影は，1.5TのMRシステム（MAGNETOM Espree, SIEMENS, Erlangen, Germa-